Original Russian Text © I. D. Rostov, E. V. Dmitrieva, N. I. Rudykh, 2022,
published in MORSKOY GIDROFIZICHESKIY ZHURNAL, Vol. 38, Iss. 1 (2022)

Interannual Variability of Thermal Characteristics in the Indian Ocean under the Conditions of Global Warming

I. D. Rostov ✉, E. V. Dmitrieva, N. I. Rudykh

V. I. Il'ichev Pacific Oceanological Institute. Far Eastern Branch of Russian Academy of Sciences, Vladivostok, Russian Federation
✉ *rostov@poi.dvo.ru*

Purpose. The purpose of this work is to clarify the tendencies and regional features of interannual changes in the surface air temperature (T_a), the sea surface temperature (SST), and the water temperature (T_w) in the upper 950-m layer in the Indian Ocean basin including the adjacent area of the Southern Ocean – up to 65°S over the past four decades, which are manifested as a result of planetary changes and a shift in the climate regime at the turn of the XX–XXI centuries.
Methods and Results. Based on the data of the Global meteorological network, reanalysis, optimal interpolation and the Global oceanographic data assimilation system GODAS (NOAA), the regional features and trends of interannual fluctuations in the water and air temperature, and their relationship with the variations in climatic indices and pressure fields in the centers of the atmosphere and wind action have been determined for the last 4 decades. The methods of a cluster, correlation, and regression analysis, and the apparatus of empirical orthogonal functions were used. The results obtained made it possible to characterize the degree of inhomogeneity of the responses of the atmosphere surface layer, SST, and vertical distribution of T_w to the ongoing global changes, to identify the isolated regions, and to quantify the rate of warming in these water areas.
Conclusions. Climatic changes in the atmosphere near-water layer and on the sea surface are expressed in positive trends (b) of changes in the SST fields and air temperature in most of the Indian Ocean basin. The values of the air temperature trends on land in the coastal areas are higher than those in the adjacent sea areas. The maximum values of the T_a trends (~ 0.5 °C/10 years) over the water area of the region are noted in the area located to the north of the Madagascar Island, and those of the SST trends (~ 0.3–0.4 °C/10 years) – in the central part of the ocean. In the T_a field, the individual areas with the minimal and negative values of T_a trends are observed in the northeastern, southwestern, and southern parts of the water area, and in the SST field – over a large area in the southern part of the ocean, namely, in the zone of influence of the cold Antarctic Circumpolar Current waters. The process of warming or cooling is significantly heterogeneous not only in space but also in time. In the upper 100-m layer of the water column, the spatial structure of the water temperature trends is rearranged. Below this layer, the maximum positive trends (on average 0.2–0.5 °C per a decade for a region) are observed in the southern and southwestern parts of the water area, and the negative ones (−0.1…−0.2 °C) – in the northwestern and southeastern parts. In course of the past 15 years, the largest relative increase of heat content in various layers occurred in the south of the ocean – it was by an order of magnitude higher than those in the other regions despite the insignificant SST trends.

Keywords: Indian Ocean, current climatic changes, regional features, water and air temperature, warming and cooling trends, climatic parameters, correlations

Acknowledgments: the work was carried out on the theme of the state task of POI FEB of RAS No. 121021700346-7. The authors thank the program developers for the opportunity to use the climatic data posted on the NOAA sites. The authors are grateful to the reviewer for the constructive comments.

For citation: Rostov, I.D., Dmitrieva, E.V. and Rudykh, N.I., 2022. Interannual Variability of Thermal Characteristics in the Indian Ocean under the Conditions of Global Warming. *Physical Oceanography*, [e-journal] 29(1), pp. 47-66. doi:10.22449/1573-160X-2022-1-47-66

DOI: 10.22449/1573-160X-2022-1-47-66

Introduction

The Indian Ocean (IO) attracts constant attention due to the peculiarities of its weather and climate conditions and its important role in ongoing global and regional climate changes [1]. A significant part (~44%) of the World Ocean's global warming occurs due to an increase in the heat content (Q) of the upper 700 m of the water column, about half of which is provided by IO [2]. So, for the 2005–2015 decade the total warming in the IO water column was more than 70% of the global increase Q [3].

The regional features of IO warming are characterized by significant spatial and temporal heterogeneity [4] and the uncertainty of quantitative estimates of the varying regime of the ocean surface temperature (SST) and its impact on the regional climate [5]. According to observations and reanalysis, from the 1970s to the beginning of the 2000s the SST in the IO tropical zone increased at a rate of ~0.1 °C per decade [6], and in the last 20 years, it has increased twice as fast, which exceeds the corresponding estimates for the Atlantic and Pacific oceans [7, 8]. This makes a significant contribution to the general upward trend in the global average SST [1, 9], affects the characteristics of monsoon circulation and currents, as well as enhances the impact of extreme weather events in the region and beyond [1, 8]. The phenomenon of a pause (*hiatus*), i.e. a slowdown in the rate of global warming [3, 10], widely discussed in previous years, is almost not expressed in the SST variation in the Indian Ocean, especially in comparison with the Pacific Ocean (PO) [11].

The interannual variability of the IO water area thermal conditions depends on the condition of the tropical warm basins (TWB) of the western part of the PO and the eastern part of the IO (*I*ndo-Pacific warm pool – IOWP [12]), in which SST is above 28 °C during the year, and on water exchange through the Indonesian Throughflow (ITF) [13]. In the PO, the costs of the western trade wind currents in the direction from east to west increase, which contributes to the formation of increased reserves of thermal energy in the western part of the PO equatorial-tropical zone. In recent decades, the area, volume, and Q of TWB have been increasing, which indicates the important role of ocean dynamics in its warming [12]. ITF is a kind of “ocean bridge” between the PO and IO. It varies on interseasonal and interannual time scales and affects variations in the thermocline depth and heat content in adjacent areas of the IO eastern part [4, 14].

The PO effect on the western part and the entire IO water area is carried out through the “atmospheric bridge” via Hadley and Walker atmospheric circulation [1, 15]. It is noted that in recent decades, after the climate regime shift of the late 1970s, the El Niño effect and ENSO (El Niño – Southern Oscillation) telecommunication with the IO western part increased [12, 16]. The occurrence of El Niño in the PO redistributes the sources of atmospheric heating, and then changes the patterns of convection and circulation in the atmosphere and can cause warming and an increase in the SST in the adjacent regions of the PO.

An analysis of half-century observational series of Q interannual variations in the upper 400 m layer showed that in the IO during 1965–1979 an increase in Q took place. During the 1980–1996 period, it was followed by its decrease, replaced by rapid growth in subsequent years [17]. We note a high correlation between variations

in heat content and thermocline depth, as well as a significant role of ITF dynamics and the wind regime of the IO and PO equatorial zone [18]. Against the background of surface water warming trends in different parts of the water area, periods of both warming and cooling of the water column at great depths [13] can be traced. This cannot be explained only by the balance of heat fluxes on the surface [19, 20] and is an urgent task of ongoing research.

In the temperate and subantarctic belts, the influence of the Southern Annular Mode (SAM) on the thermal conditions of the IO is pronounced [4, 8]: the SAM reflects the zonality of air mass transfer in temperate and high latitudes as the main characteristic of atmospheric processes and manifests itself in variations of many climatic variables. An indicator of the increase or decrease in the intensity of zonal transport is the Antarctic Oscillation index (AAO), which reflects anomalies in the annular circulation of the atmosphere around the South Pole [21]. One of the main features of modern changes in the regime of climatic characteristics in the subantarctic IO belt is the AAO shift to the region of positive values, the strengthening of westerly winds, and the poleward shift of the SAM [22, 23]. Poleward strengthening westerly winds lead to a meridional dipole structure of changes in wind stress vorticity over moderate and high latitudes. In accordance with the changing winds, there has been an increase and expansion to the pole of the subtropical oceanic circulations of the Southern Hemisphere (SH) [23]. The heat absorption by the ocean surface mainly occurs in the region of the frontal zones of the high latitudes of the South Pacific region with a global average maximum in ~ 58°S zone, where the rising cold waters come to the surface and meet with a warmer atmosphere [24]. About two-thirds of the heat absorbed in the Southern Ocean is removed by advection along the inclined isopycnal surfaces to the intermediate layers to the north and accumulates in middle latitudes [25], while the deepest warming occurs at the boundary between subtropical gyres and the Antarctic Circumpolar Current (ACC) [23]. It is noted [26] that as a result of subduction, Ekman pumping, and downwelling, an increase in the volume of subantarctic modal water in the subpolar and subtropical regions and an increase in the heat content of the upper and intermediate layers of the IO extratropical zone are observed. It is assumed that modal waters (due to their ability to accumulate heat) can play a key role in climate regulation [26].

In some works, the characteristics of the temperature trend vertical structure were considered on the scale of the entire IO basin [2, 27]. It is shown that warming is accompanied by a deepening of isotherms and isopycnal surfaces and leads to the “swelling” of isopycnals. In the southern part of the subtropical gyres of the SH, this depression reaches almost 100 m in 50 years [2, 28]. According to the estimates of trends in heat content changes in different layers based on the data of Argo floats, in the structure of field *Q*, it is possible to distinguish individual “hot spots” and “cold spots” covering areas of intense vertical mixing and associated with the formation of surface and intermediate waters [2].

The regional features of the IO weather and climate conditions are largely determined by the monsoon regime and the interaction of baric formations, which are permanent or seasonal atmospheric centers of action (ACAs) [1, 4, 29].

Interannual SST fluctuations in the IO demonstrate long-range relationships with the variations in climatic parameters in the Atlantic and PO, estimated by AMO, IPO, SOI, PDO indices, etc. [14, 15, 17]. However, the nature and structure of these relationships within the ocean basin itself require further study.

The purpose of this work is to clarify the trends and regional features of interannual changes in the surface air temperature (T_a), SST, and water temperature of the upper 950-meter layer in the Indian Ocean basin with the adjacent latitudinal belt of the Southern Ocean (up to 65°S) over the past decades, manifested as a result of planetary changes and a shift in the climatic regime at the turn of the 20th– 21st centuries.

Data and methods

Air temperature observations (T_{ac}) were used at 76 coastal weather stations (WS) of the global climate network GHCN-M (V3) NOAA (https://www.ncdc.noaa.gov/ghcnm/v3.php) over 1978–2020 period, as well as grid data of temperature reanalysis (T_a – NCEP/NCAR Reanalysis-1), pressure fields, wind, heat fluxes on the ocean surface and climate indices (CI) [30]. The considered CIs have a certain geographical reference and physical interpretation (https://climatedataguide.ucar.edu/climate-data). The listed data was obtained from the website https://psl.noaa.gov/data/gridded/index.html of its developer: NOAA/ESRL/Physical Sciences Laboratory (PSL), Boulder, Colorado, USA and from the websites of NOAA/NCEI/CPC https://www.nodc.noaa.gov/ and https://www.cpc.ncep.noaa.gov/. We also used the IO dipole index – DMI (https://psl.noaa.gov/gcos_wgsp/Timeseries/DMI/) and the intensity indicators of regional ACAs – Mascarene and Antarctic maxima (MM, AM), Australian, Indian Ocean lows (AVM, IM) and Asian depression (AD) [29].

To analyze the interannual fluctuations in water temperature, we used the data of the optimal SST interpolation – NOAA OI SST V2 for 1982–2020 from the site https://www.esrl.noaa.gov/psd/ and the data on potential water temperature (T_w) and currents at different horizons of the GODAS oceanographic data assimilation system from the site https://www.esrl.noaa.gov/psd /data/gridded/data.godas.html for 2005–2020. In the 2000s, in the area under study, the share of information entering the GODAS system from the observation network of floats increased significantly: from 628 profiles in 2001 [31] to 481.4 thousand profiles in 2005–2020 under conditions of full coverage of the water area, including areas where the observations from vessels are not carried out.

A unified method of statistical processing of the data used [30, 32], supplemented by a regression analysis of the set of climatic variables, was applied. Taking into account the nature of the monsoons, conditionally warm (November–March) and conditionally cold (June–October) seasons (periods) of the SH year were identified.

Applying the SST data by cluster analysis methods for three main components *, four separate regions located in different climatic zones were identified in the IO basin: northwestern (NW), southwestern (SW), southeastern (SE), and southern (S) (Fig. 1, *b*). Subsequently, by simple averaging of grid data, the long-term variation of water and air temperature within the boundaries of each region was calculated.

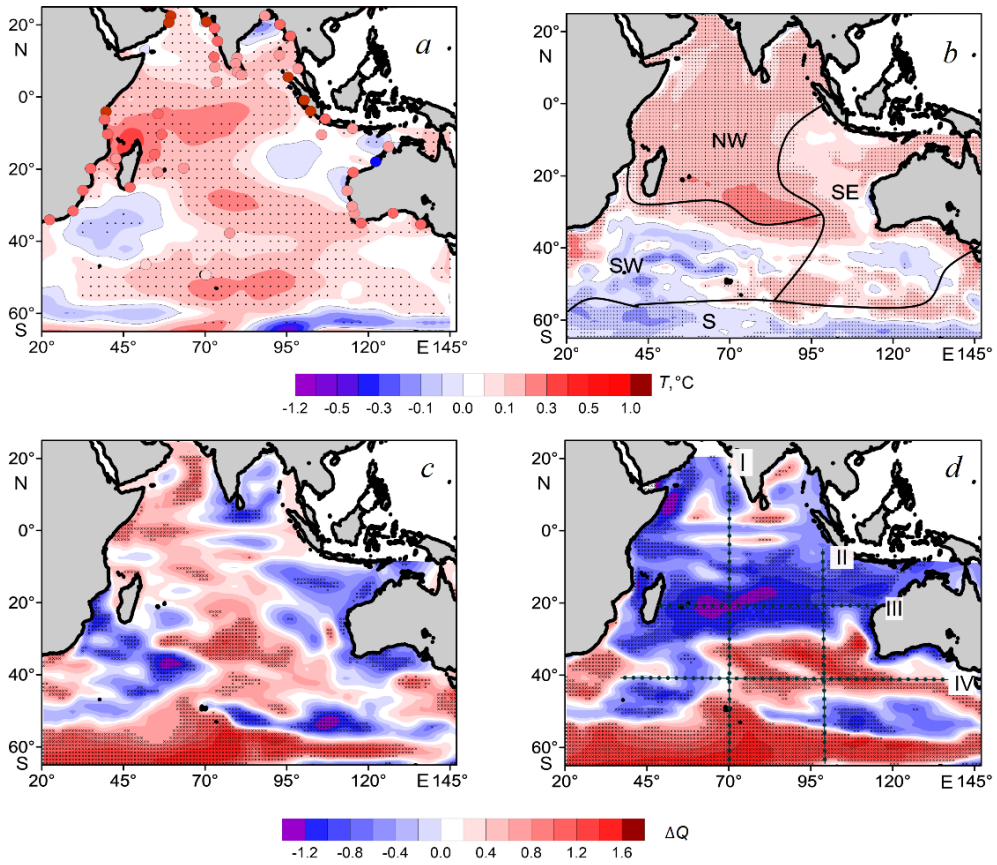

F i g. 1. Trends (°C/10 years) of the annual average values of T_a, T_{ac} (*a*), SST (*b*) and the normalized heat content anomalies in the layers 5–300 m (*c*) and 300–750 m (*d*) based on the data of reanalysis, observations at meteorological stations and *GODAS*. Shown are the locations of meteorological stations (*a*), selected areas (*b*), and individual sections (*d*). Here and below, dots denote the grid nodes in which the estimates are statistically significant at the 95% level

In the Southern Region, most of which is located southwards of 50ºS, there are southern subarctic, northern subarctic, and polar frontal zones [24].

* Ding, C. and He, X., 2004. K-means Clustering via Principal Component Analysis. In: ICML, 2004. Proceedings of the Twenty-First International Conference on Machine Learning (ICML '04). Banff, Alberta, Canada: ACM Press, 29. doi:10.1145/1015330.1015408

Features of spatial and interannual variability of air temperature and SST

In the atmospheric near-water layer and on the sea surface, the warming trends over the past four decades are expressed in positive trends (*b*) of changes in the SST fields and air temperature over most of the water area.

The maximum values *b* of air temperature T_{ac} > 1.0 °C/10 years are traced according to observations at separate weather stations located in the coastal and insular zones of the tropical belt. According to the reanalysis data, the maximum values of T_a trends (~ 0.5 °C/10 years for 1978–2020) over the region's water area are observed in the NW region northwards to the island of Madagascar, while the SST trends (~ 0.3–0.4 °C/10 years for 1982–2020) are in the IO central part. In general, the values of air temperature trends on the land are somewhat higher than in adjacent marine areas. Areas with minimal and negative values of *b* in the SST field are observed mainly in the southern part of the IO only – in the zone of the effect of the ACC cold waters.

As in other areas [32], the features of spatial-temporal variability of water temperature trends at different horizons and heat content in individual layers (Fig. 1, *c*, *e*) differ from the characteristics of the SST trends (they will be considered below). Table 1 contains generalized quantitative estimates of the trends in ongoing changes in T_a, T_{ac}, and SST on average for the regions over a year and in individual seasons.

The largest values of T_a and SST trends (as well as their contribution to the total dispersion D), which correspond to a warming of 0.5 °C during the period under study, were observed in the northwestern part of the IO, and the smallest and statistically insignificant ones – in the southern part. In two regions (NW and SE), where T_a and SST fluctuations are characterized by closer correlations (*R*), the trends of both parameters are statistically significant. In general, in the region, the air temperature increased approximately 1.3 times faster than the SST, especially in the adjacent areas of the coastal zone. During the period under consideration, T_a over the water area increased by about 0.3 °C, SST – by 0.2 °C, which is consistent with the corresponding estimates for the adjacent regions of the Pacific Ocean southern part [32]. At the same time, seasonal differences in the warming rate estimates are better expressed in T_a field than in the SST one (Table 1).

The interannual changes in the mean annual anomalies of T_a, SST, and the accumulated anomalies within the NW and SE regions, where moderate correlations between these characteristics are expressed (Table 1), are identical (Fig. 2), while in other regions they differ only in details.

The integral curves of accumulated anomalies correspond to individual phases of the alternation of warm and cold years and periods, which, as will be shown below, are consistent with the changes in individual CIs and regional ACAs. The variation of these curves (Fig. 2, *e*, *f*, *g*, *h*) reflects both the internal features of these relationships and the inhomogeneous nature of the warming process in the atmosphere and on the ocean surface in space and time. Distinctive features of the anomaly accumulation process are more noticeable when comparing the SST variability in the southern and northwestern regions, in which SST trends of different signs were observed (Fig. 2, *e*, *h*).

Table 1

Trends of interannual changes of the SST anomalies (1982–2020) and the air temperature (1978–2020) based on the reanalysis data (T_a) and the observations at 76 MS (T_{ac}) in the identified domains

Area	Parameter	*b*	*D*	*tr*	b_w	b_c	*R*
NW	T_a	**0.12**	38	0.5	**0.14**	**0.10**	**0.57**
	SST	**0.13**	48	0.5	**0.13**	**0.13**	
SW	T_a	**0.08**	26	0.4	**0.07**	**0.08**	0.13
	SST	0.04	5	0.1	0.06	0.01	
SE	T_a	**0.06**	12	0.3	0.03	**0.07**	**0.58**
	SST	**0.07**	12	0.3	0.06	**0.06**	
S	T_a	0.05	3	0.2	**–0.08**	0.15	0.27
Whole area	T_a	**0.08**	32	0.3	**0.04**	**0.10**	**0.69**
	T_{ac}	**0.19**	–	0.8	**0.19**	**0.20**	
	SST	**0.06**	31	0.2	**0.06**	**0.05**	

N o t e. *b* is the slope coefficient of the average annual temperature linear trend, °C for 10 years; D is the trend contribution to the total variance, %; *tr* is the trend over the observation period, °C; $b_т$, b_x are the values of *b* for the warm and cold seasons; *R* is the correlation coefficient of the average annual SST and T_{ac}. Here and in Table 2, the statistically significant (95%) estimates of the trends and the correlation coefficients are highlighted in bold

In the years corresponding to the pause in global warming, when in 2002–2012 the SST increase generally continued [11] and an "interhemispheric gradient" of the SST trends appeared [14, 33], according to our estimates, there was a slight decrease in the magnitude of positive trends in the average annual SST in the NW and SW regions, their fourfold increase in the region of SE, and an increase in negative trends in Southern area. In general, in the water area of the IO, as a result of the strongest warming in the SE region, this value (~ 0.09 °C/10 years) turned out to be even somewhat higher than for the entire period under consideration (Table 1). It roughly corresponded to the estimates obtained using other data and differed significantly from global trends (–0.03 °C/10 years) [11]. The interannual variability of the IO thermal conditions during this period was largely determined by the features of the interbasin interaction of the Pacific and Indian oceans and was associated with

an increase in the ITF costs by 0.9–1.0 Sv/10 years [11, 14], resulting in a redistribution of heat between the upper layers of these oceans through the "ocean bridge". The studies have shown that the ITF heat transfer increased in the early 2000s under effect of a series of long-term La Niña events against the background of El Niño weakening [33] with the strengthening of the easterly trade winds. These events were accompanied, respectively, by an increase or decrease in the heat content of waters in the southeast of the IO in the first decade of the 21st century and occurred during the positive phase of SOI and the negative phase – interdecadal oscillation (IPO) [34]. They are considered as one of the causes explaining the slowdown in the increase of global surface temperature, and their mechanisms are well studied, for example in [17]. According to the Japan Meteorological Agency (JMA) (https://www.data.jma.go.jp/gmd/cpd/data/elnino/learning/faq/elnino_table.html), during the 2000–2012 period 12 La Niña seasons and only 7 El Niño seasons took place. At the same time, a statistically significant trend of an increase in the easterly trade winds velocity in the equatorial western part of the Pacific Ocean (135–180°E), contributing to an increase in heat transfer to the Indian Ocean of the ITF and the strongest warming in the SE region, amounted to ~ 0.2 m/s in a year.

At the same time, separated years of the period under study, when the maxima (1982, 1986–1987, 1998, 2003, 2010, 2015) or minima were expressed in the alternation of average annual SST values in the IO water area, fully corresponded to the phases of El Niño and La Niña manifestations due to the "atmospheric bridge". For instance, according to the JMA and other studies, in 2015, when the largest positive anomaly in the Indian Ocean mean SST in recent decades (0.24 °C) was noted, one of the most powerful El Niño events was observed. It was comparable in strength to similar events in 1982–1983 and 1997–1998 and caused significant temperature anomalies and changes in atmospheric circulation outside the Pacific Ocean tropical zone [35]. These changes led to a deepening and shift of the maximum positive SST anomaly focus near the equator from the South America coast to the west. In this situation, anomalously warm conditions were also observed over the central part of the IO and in the adjacent areas. Positive temperature anomalies were due to the radiation factor: under El Niño conditions, powerful cloudiness caused by intense convection shifted eastward following the tongue of warm water, and insolation over Indonesia and the Indian Ocean increased, which led to an increase in surface temperature [35].

To obtain generalized information about the structure of spatial-temporal variations in the SST and T_a fields, empirical orthogonal functions (EOFs) of interannual fluctuations in the anomalies of these parameters, as well as anomalies in the geopotential field of 500 hPa (ΔH_{500}) isobaric surface in the middle troposphere, were calculated. In Fig. 3, the spatial distribution of the obtained EOFs is presented as fields of correlation coefficients between the principal components (PC), or temporal expansion coefficients of the fields in terms of EOFs (K), and the series of these parameters at each point [32].

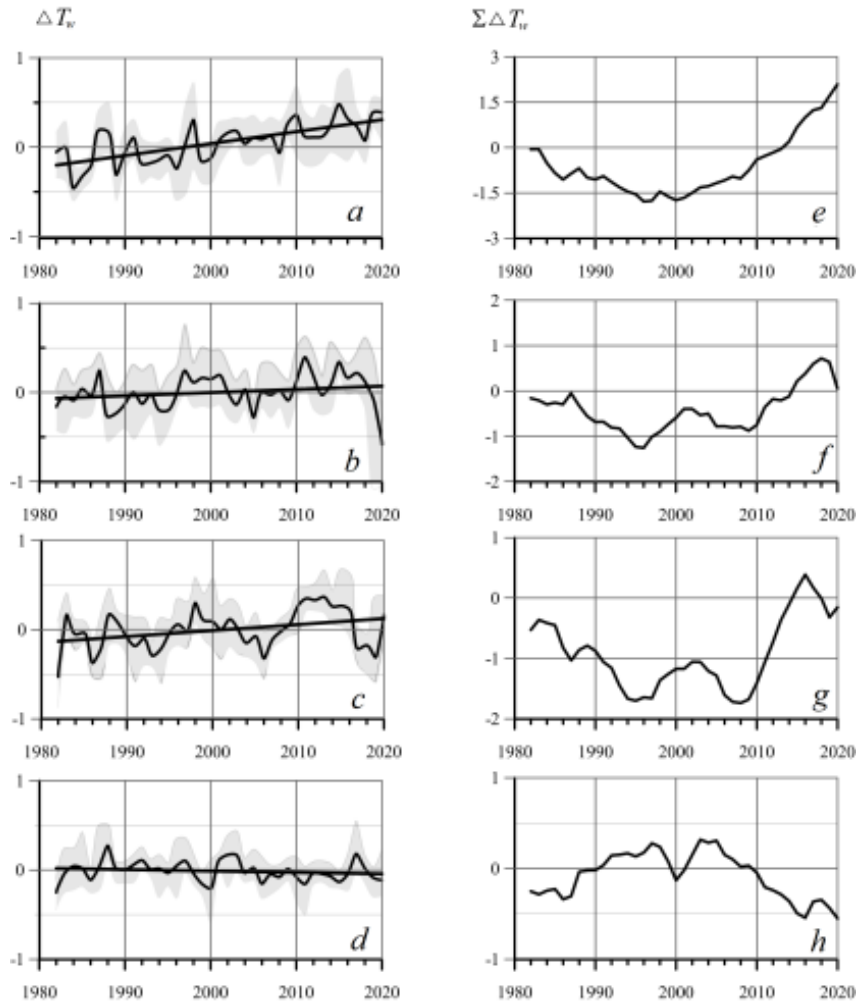

F i g. 2. Interannual variability of the annual average SST anomalies (ΔT_w) and the cumulative anomalies $\sum\Delta T_w$ in the identified domains: NW (*a*, *e*); SW (*b*, *f*); SE (*c*, *g*) and S (*d*, *h*). The range of intra-year fluctuations, the mean values in the region, and the linear trend (bold lines) are shown

The fields of correlation coefficients (Fig. 3) characterize mainly antiphase fluctuations of T_a, SST, and H_{500} anomalies within water areas described by different modes. The first SST EOF mode (Fig. 3, *d*) corresponds to the leading regime of the Indian Ocean basin and is mainly associated with the external effect of El Niño – Southern Oscillation and other large-scale processes. In the chosen coordinate system, the dipole regime of the IO tropical sector [36] is expressed in the second mode of the EOF SST, and the subtropical dipole [37] is expressed in the third mode (Fig. 3, *e*, *f*). The first mode of geopotential fluctuations reflects the dominant annular regime of pressure field variability, thermal conditions, and zonal winds and currents in the SP [38]. It, as well as the second mode of the EOF H_{500}, is closely related to the state of the main regional ACA and interannual variations in the PCs of the fields of the EOF T_a (Table 2) and SST.

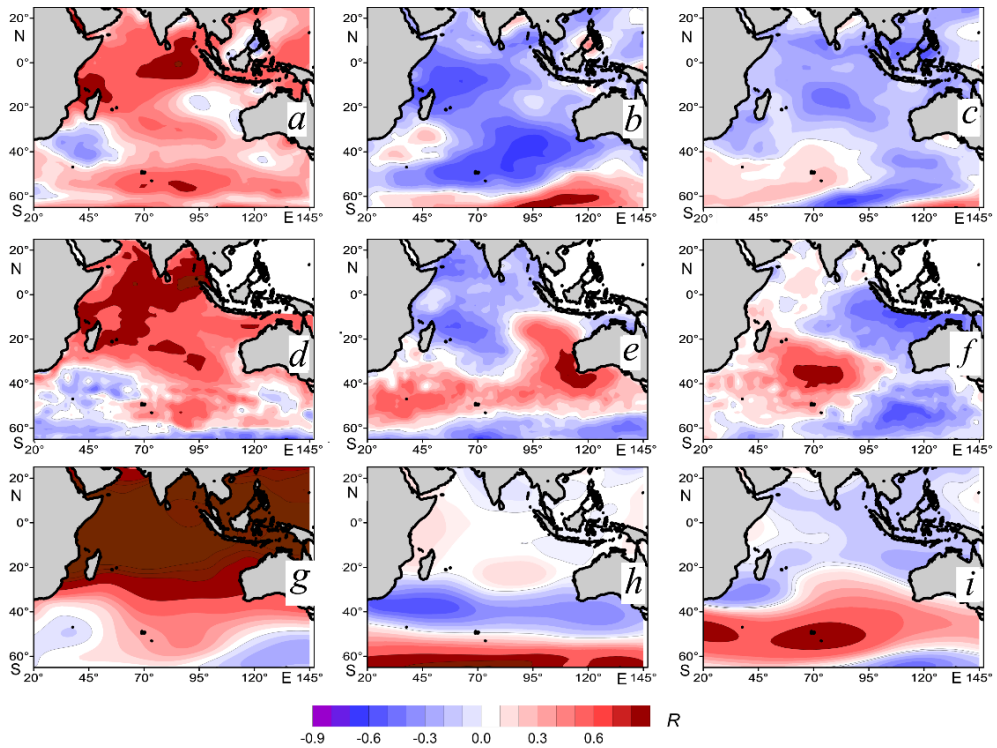

F i g. 3. Fields of the first, second and third EOF modes of the average annual temperature anomalies T_a (*a*, *b*, *c*), SST (*d*, *e*, *f*) and the normalized anomalies H_{500} (*g*, *h*, *i*)

T a b l e 2

Correlation coefficients between the fluctuations of the surface atmospheric pressure fields in ACA and the EOF coefficients (*K*) of the first EOF modes ΔH_{500} and ΔT_a for the warm (w) and cold (c) seasons of the SH in 1978–2020

EOF	$K_1\ \Delta H_{500}$		$K_2\ \Delta H_{500}$		$K_3\ \Delta H_{500}$	
	w	c	w	c	w	c
AVM	**0.5**	–	0.3	–	–0.1	–
MM	0.1	0.3	–0.2	**–0.7**	**0.4**	0.1
AM	–0.1	**–0.5**	**0.5**	**0.4**	–0.1	–0.3
IM	–0.1	**–0.4**	**0.7**	**0.4**	**0.5**	0.3
AD	–	**0.3**	–	**–0.5**	–	–0.1
$K_1\ \Delta T_a$	**0.8**	0.1	0.0	**0.7**	**0.8**	0.2
$K_2 \cdot \Delta T_a$	–0.3	0.0	**0.5**	0.1	–0.2	0.2
$K_3\ \Delta T_a$	**-0.3**	**–0.5**	**–0.6**	**–0.3**	–0.2	0.3

N o t e. Dash means the absence of the ACA in a given season.

The main features of the expansion coefficients' spatial distribution of the first C_1 EOF modes of T_a and SST anomalies (Fig. 3, *a*, *d*) agree satisfactorily with the distribution of the trends' values of these climatic variables (Fig. 1, *a*, *b*).

Temperature variability of subsurface and intermediate layers

In order to analyze regional features and estimate the interannual variability of T_w and Q at different horizons and layers, we used GODAS grid data on 31 horizons in 5–950 m layer for each month of the year for 2005–2020 period and previously tested methodological approaches [32]. In Fig. 4 the curves of T_w vertical distribution, the range of its variability, and the temperature trend at different horizons averaged within the selected areas, are demonstrated.

The maximum values of seasonal variations in T_w average annual values were observed at near-surface horizons in the SW area (2.8 °C) and decreased to 1.9–2.2 °C in other regions (Fig. 4, *a* – *d*), and within each of the seasons did not exceed 0.8–1.7 °C, reaching the maximum values in the warm period of the year. Below 100–200 m layer, the range of seasonal values decreases nonmonotonically with depth (Fig. 4, *e* – *h*). The relationship between temperature changes at different horizons is manifested in the vertical profiles of T_w trends (Fig. 4, *i* – *l*). The magnitude and sign of trends in individual layers of the water column in the warm and cold seasons change quasi-synchronously, reaching the maximum values (0.2–0.5 °C per decade) in the warm period of the year. These values are 2–5 times higher than on the ocean surface (Table 1) and correspond to similar estimates for the Pacific Ocean southern part. In the SW and S regions the prevailing trend is the warming of the entire water column in the considered depth range, while in the other two regions – cooling below 100–200 m. As noted earlier [32], the obtained results reflect only general trends and characteristics of T_w interannual changes of the studied water area in the selected period of time, taking into account the assumption that the studied GODAS fields correspond to real conditions. Estimates of relative changes in the integral heat content (Q) in layers 5–300, 300–750, 5–950 m for 2005–2020 were made using these data. In the southern part of the ocean (S region), despite the absence of statistically significant SST trends, the value of relative changes Q in the water column is an order of magnitude higher than in other areas: by 18% (up to 27%) with a maximum in the upper layer, as observed and in the South Pacific [32]. In this area, a monotonous increase in Q in all layers occurred over the entire 15-year period, while in other parts of the water area this process was non-uniform in time. The rapid growth of Q in NW, SE, and SW regions in the first decade of the 20th century was replaced by a sharp heat content decrease in all layers in subsequent years, due to which the total value of relative changes in Q in all layers did not exceed ±3%.

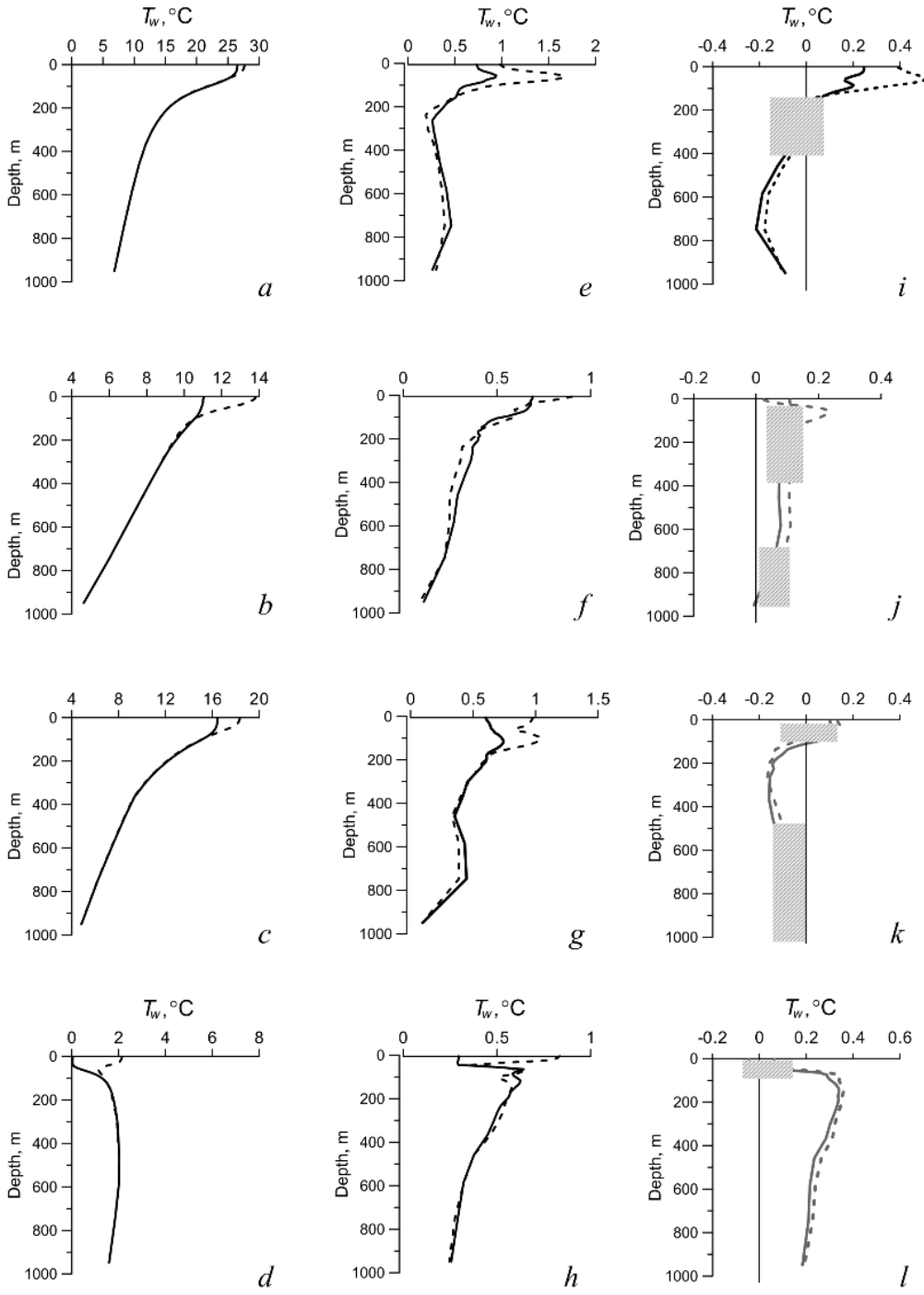

F i g. 4. Generalized curves of vertical distribution (*a*, *b*, *c*, *d*), range of changes (*e*, *f*, *g*, *h*), and T_w trend (*i*, *j*, *k*, *l*) in the warm (dotted line) and cold (solid line) seasons in 2005–2020. From top to bottom: the areas NW, SW, SE, S. The layers with the trend insignificant at the 95% level are shaded

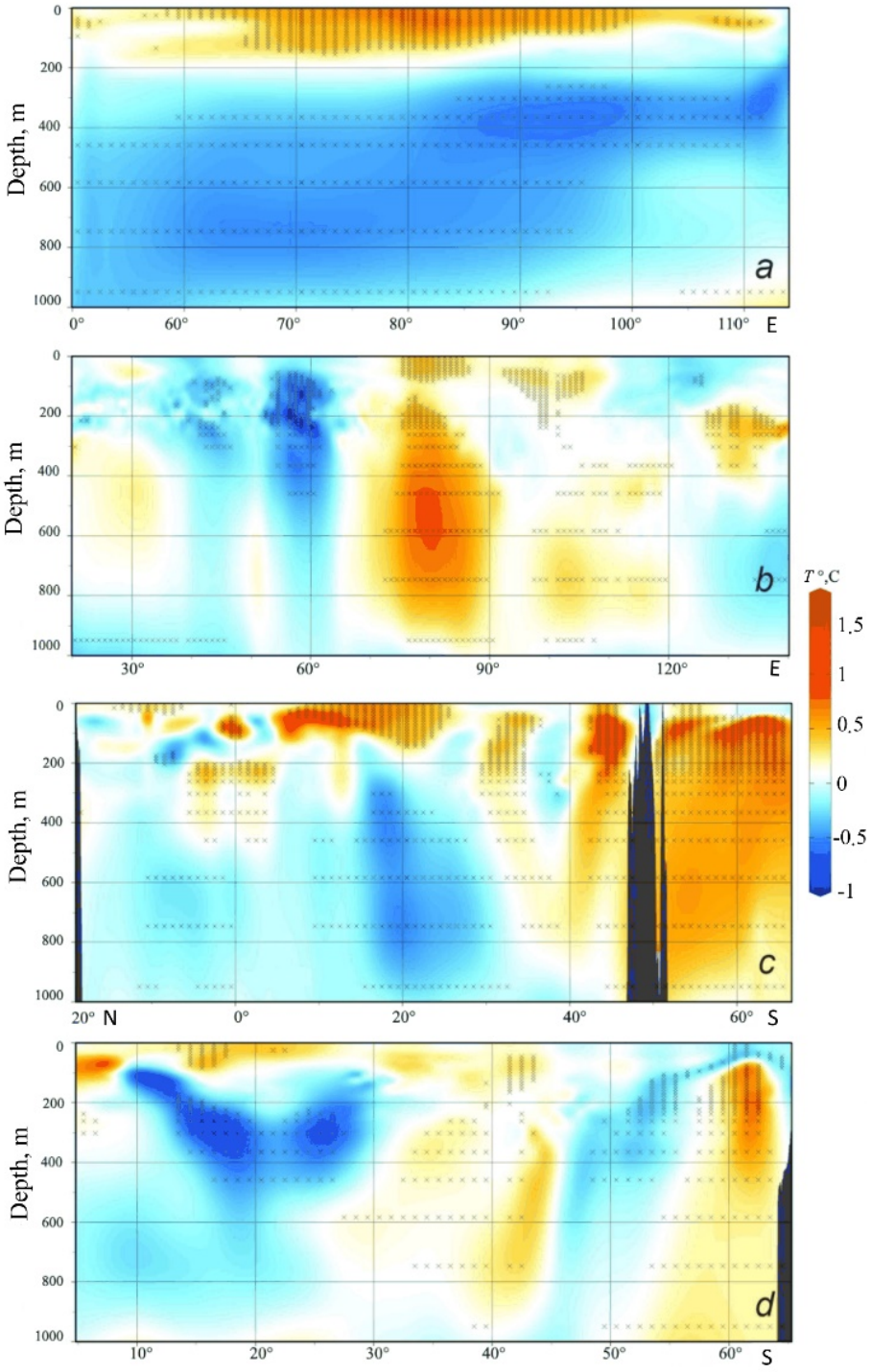

F i g. 5. Variability of the trends in the average annual T_w on the zonal III, IV (*a*, *b*) and meridional I, II (*c*, *d*) sections location of which is shown in Fig. 1, *d*

Figures 1, *c*, *e*; 4 and 5 give a general idea of Q and T_w variation trends in 5–950 m layer in different parts of the IO water area. During the period under study, a steady increase in the heat content of this entire layer was observed in the southern part of the IO. For the central and northern parts of the water area, the prevailing trend was the warming of the upper layer of the ocean, while the intermediate layers, especially in the tropical and subtropical zones, are subject to cooling.

As demonstrated above, the upper layer warming in latitudinal section III, located at the southern boundary of the South Equatorial Current, as well as in sections of meridional sections I and II between 10ºS and 25ºS (Fig. 5, *a*, *c*, *d*) crossing this area can be associated with the effect of Tropical Warm Pools (TWPs) and increased ITF heat transfer, while most of the SST variability is associated with the surface heat fluxes [5]. A significant effect on the formation of the vertical structure of temperature trends is exerted by the wind field stress and vorticity associated with ongoing changes in the characteristics of atmospheric circulation [14, 17]. In the temperate and subantarctic belts of the southern part of the IO (Fig. 5, *b* – *d*), the deepest warming is observed in the subsurface and intermediate layers along the boundary between the subtropical gyre and the ACA [23, 26], as well southward. As noted above, the SAM effect on thermal conditions is pronounced in this region [4, 8]: the SAM shift towards the pole and strengthening of westerly winds [22], the formation of a dipole structure of wind stress vorticity over moderate and high latitudes. Here, the thermodynamic effect on the ocean surface becomes aggravated, and the volume of subduction of subantarctic modal and antarctic intermediate waters propagating northward from the subantarctic and south polar fronts increases [24, 32]. According to our estimates, in the IO latitude band 40–60ºS there were observed the trends towards the increase in the average annual values of the westerly wind velocity by about 0.3–0.4 m/s per decade, and southward of 65–80ºS, in separate centers off the coast of Antarctica, – easterly winds by the same value. Between these areas, a band with the largest horizontal gradients of the height of 500 hPa isobaric surface geopotential, due to a change in the trend sign of this parameter, was located. At the same time, over most of the water area in the band ~ 50–65ºS positive (anticyclonic in SH) values of the wind field vorticity, contributing to the intensification of downwelling and the deepening of the thermocline [12, 14], were observed. Earlier it was noted that at the boundary of this area, approximately at 45–50°S, one of the centers of sign change of vorticity and maximum wind stress [39] was located.

Pronounced warming in the IO latitude band 40–50°S spreading up to 800 m and more (Fig. 1, *d*; 5, *c*, *d*), can be explained by the expansion and southward displacement of the subtropical circulation as a result of increased westerly winds [22, 40]. In the upper layer northward of this area, another area of warming is observed, and deeper than it, there is an area of extensive cooling of subsurface layers (Fig. 1, *d*; 5, *a*, *c*, *d*). The formation of these anomalies is associated with the strengthening of the southern subtropical circulation cell in the atmosphere during the onset of the negative phase of ITF and positive DMI [13, 22].

A cross-correlation and regression analysis of the time series of SST anomalies with fluctuations in the anomalies of the geopotential field of 500 hPa isobaric surface, atmospheric pressure in the ACA, and climatic indices characterizing the state and dynamics of the climate system in the study areas was carried out. The features and nature of the corresponding relationships, reflecting the influence

of various large-scale processes on the thermal conditions of individual areas of the IO water area, are expressed in the field of spatial distribution of linear regression coefficients of the variability of SST characteristics and fluctuations of various indices (Fig. 6).

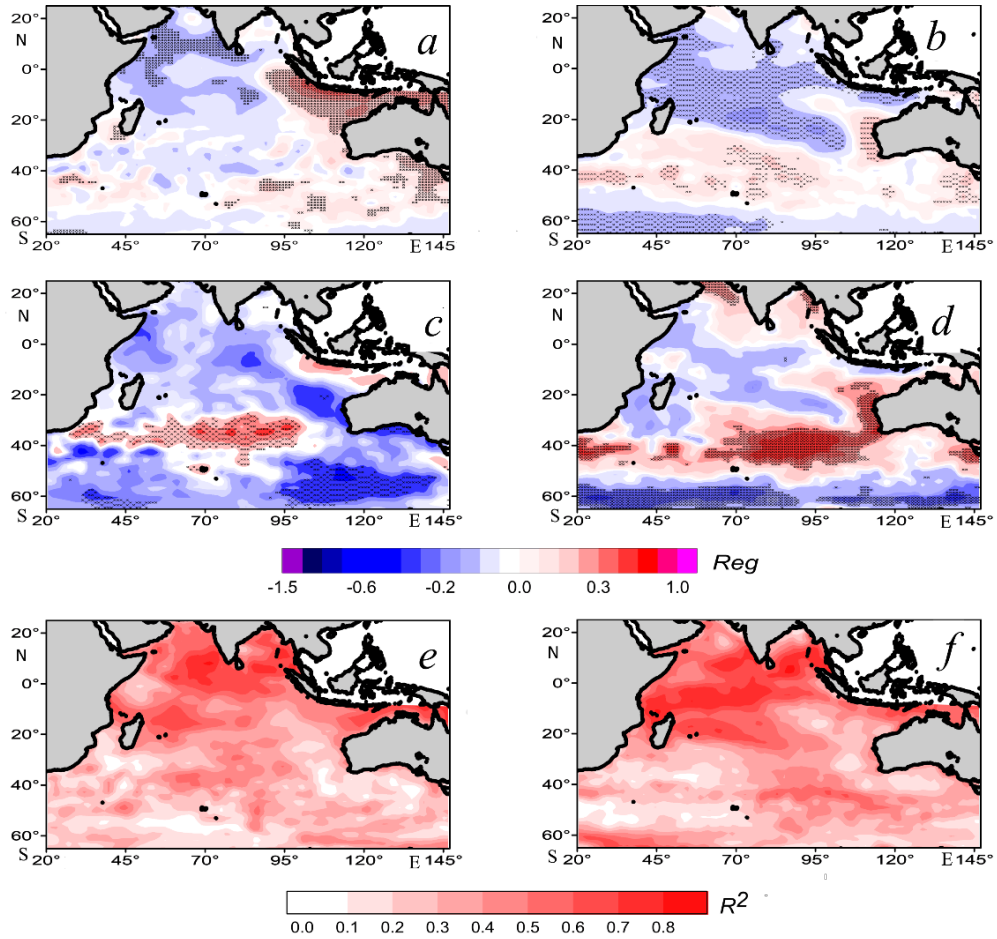

F i g. 6. Linear regression coefficients (*Reg*) of the SST fluctuations with the climatic indices: *SOI* (*a*, *b*), *AAO* (*c*, *d*) in the cold (left) and warm (right) seasons. The distribution of the determination coefficients R^2 of the SST multiple regression and 7 different indices (*e*, *f*) is also shown

The analysis demonstrated that the most significant (simultaneously in two or more areas of the water area) statistically significant correlations were manifested for the following CIs: AMO, AAO, SOI, PTW, IPO, PWP, as well as for the severity of individual ACA – Mascarene, Antarctic maxima, Australian minimum (MM, AM, AUM) and EOF ΔH_{500}. The SST relationships with variations of the DMI index are expressed only in the NW region. In Fig. 6, *e*, *f* the distribution of the corresponding values of the coefficient of R^2 determination of the multiple regression of these variables and SST was revealed.

In Table 3 the values of the explained dispersion (*D*, %) of the multiple regression of the contribution of the totality of fluctuations of individual climate

indices (SOI, AAO, PTW, AMO) and the first one – the third EOF ΔH_{500} modes to the SST variability in different regions for the warm (w) and cold (c) 1982–2020 seasons.

Table 3

Percent of the explained variance (D, %) of the contribution of climatic variables combination to the SST variability in different areas

Area	D, %	
	w	c
NW	88	79
SW	35	48
SE	49	41
S	34	20

Using the GODAS data, statistically significant correlations ($R > |0.51|$) of water temperature fluctuations in individual layers of the water column with trends in individual CI changes were revealed. Within the upper active layer in the NW region, these relationships are expressed with SOI, PWP, $K_1\ \Delta H_{500}$, $K_3\ \Delta H_{500}$ indices in the warm season and with $K_1\ \Delta H_{500}$ in the cold season; in the SW region, with PWP and $K_3\ \Delta H_{500}$ during the warm period and with the AAO and $K_3\ \Delta H_{500}$ during the cold period. In the SE and S regions, these relationships are mainly expressed only with the AAO indices $K_1\ \Delta H_{500}$ and $K_1\ \Delta H_{500}$. The features of the spatial distribution of the corresponding correlation coefficients in the 5–100 m layer generally agree with the corresponding characteristics of the connections on the water area surface. At the same time, in the underlying layers, the nature of the relationships between the T_w and CI fluctuations significantly changes, up to a change in the sign of the correlation coefficients, which is due both to the identified features of the vertical structure of the temperature trend field (Fig. 4, 5) and the influence of a large number of the work of factors. These results require further analysis in a separate work.

Conclusion

In the last four decades, in the atmospheric near-water layer and on the sea surface the warming trends are expressed in positive trends (b) in changes in SST and T_a fields over most of the Indian Ocean basin. According to the reanalysis data, during this period, the maximum values of T_a trends (~ 0.5 °C/10 years) over the water area of the region are observed in the area located northward of the island of Madagascar, SST trends (~ 0.3–0.4 °C/10 years) are in the central part of the ocean, and the minimum and negative ones are in the southern part of the ocean. In general, in the Indian Ocean basin region, over the past 40 years, the air temperature over its water area has increased by about 0.3 °C, the SST – by 0.2 °C,

which is consistent with the corresponding estimates for the Pacific Ocean southern part.

Over the past 15 years, the prevailing trend in the southern and southwestern regions of the water area has been the warming of the entire water column in the considered depth range from 5–10 m to 950 m, while in other areas – cooling below 100–200 m. The largest relative increase in heat content in different layers occurred in the south of the ocean area – an order of magnitude more than in other areas, despite the negative SST trends.

Due to the peculiarities of the inter-basin interaction of the Pacific and Indian Oceans, the phenomenon of slowing down the rate of global warming in the first decade of the 21st century during the SST of the area under study is not clearly expressed. On the contrary, it was during this period that a rapid increase in the heat content of the water column was observed in all regions of the Indian Ocean, which provided a significant part of the global increase in Q. In recent years, the opposite trend has been observed.

The effect of various large-scale processes on the structure of pressure fields, winds, and thermal conditions in various regions of the Indian Ocean manifests itself most extensively through the correlations of these parameters with the climate indices AMO, AAO, SOI, PTW, IPO, PWP, as well as with the severity of individual ACA – Mascarene and Antarctic maxima, Australian minimum and EOF of the field of geopotential anomalies ΔH_{500}.

The alternation of warm and cold periods in the interannual variation of averages over the entire SST basin completely corresponded to the phases of El Niño and La Niña manifestations in the Pacific Ocean.

REFERENCES

1. Gnanaseelan, C., Roxy, M.K. and Deshpande, A., 2017. Variability and Trends of Sea Surface Temperature and Circulation in the Indian Ocean. In: M. Rajeevan and S. Nayak, eds., 2017. *Observed Climate Variability and Change over the Indian Region*. Singapore: Springer, pp. 165-179. doi:10.1007/978-981-10-2531-0_10
2. Desbruyères, D., McDonagh, E.L., King, B.A. and Thierry, V., 2017. Global and Full-Depth Ocean Temperature Trends during the Early Twenty-First Century from Argo and Repeat Hydrography. *Journal of Climate*, 30(6), pp. 1985-1997. doi:10.1175/JCLI-D-16-0396.1
3. Lee, S.-K., Park, W., Baringer, M.O., Gordon, A.L., Huber, B. and Liu, Y., 2015. Pacific Origin of the Abrupt Increase in Indian Ocean Heat Content during the Warming Hiatus. *Nature Geoscience*, 8, pp. 445-450. doi:10.1038/ngeo2438
4. Schott, F.A., Xie, Sh-P. and McCreary Jr., J.P., 2009. Indian Ocean Circulation and Climate Variability. *Reviews of Geophysics*, 47(1), RG1002. doi:10.1029/2007RG000245
5. Li, Yu., Han, W., Zhang, L. and Wang, F., 2019. Decadal SST Variability in the Southeast Indian Ocean and Its Impact on Regional Climate. *Journal of Climate*, 32(19), pp. 6299-6318. doi:10.1175/JCLI-D-19-0180.1
6. Roxy, M.K., Gnanaseelan, C., Parekh, A., Chowdary, J.S., Singh, Sh., Modi, A., Kakatkar, R., Mohapatra, S., Dhara, Ch., Shenoi, S.C. and Rajeevan, M., 2020. Indian Ocean Warming. In: R. Krishnan, J. Sanjay, C. Gnanaseelan, M. Mujumdar, A. Kulkarni and S. Chakraborty, eds., 2020. *Assessment of Climate Change over the Indian Region*. Singapore: Springer, pp. 191-206. doi:10.1007/978-981-15-4327-2_10
7. Blunden, J. and Boyer, T., 2021. State of the Climate in 2020. *Bulletin of the American Meteorological Society*, 102(8), pp. S1-S475. doi:10.1175/2021BAMSStateoftheClimate.1

8. Luffman, J.J., Taschetto, A.S. and England, M.H., 2010. Global and Regional Climate Response to Late Twentieth-Century Warming over the Indian Ocean. *Journal of Climate*, 23(7), pp. 1660-1674. doi:10.1175/2009JCLI3086.1

9. Roxy, M.K., Ritika, K., Terray, P. and Masson, S., 2014. The Curious Case of Indian Ocean Warming. *Journal of Climate*, 27(22), pp. 8501-8509. doi:10.1175/JCLI-D-14-00471.1

10. Nieves, V., Willis, J.K. and Patzert, W.C., 2015. Recent Hiatus Caused by Decadal Shift in Indo-Pacific Heating. *Science*, 349(6247), pp. 532-535. doi:10.1126/science.aaa4521

11. Arora, A., Rao, S.A., Chattopadhyay, R., Goswami, T., George, G., Sabeerali, C.T., 2016. Role of Indian Ocean SST Variability on the Recent Global Warming Hiatus. *Global and Planetary Change*, 143, pp. 21-30, doi:10.1016/j.gloplacha.2016.05.009

12. Rao, S.A., Dhakate, A.R., Saha, S.K., Mahapatra, S., Chaudhari, H.S., Pokhrel, S. and Sahu, S.K., 2012. Why is Indian Ocean Warming Consistently? *Climatic Change*, 110(3–4), pp. 709-719. doi:10.1007/s10584-011-0121-x

13. Ummenhofer, C.C., Biastoch, A. and Böning, C.W., 2017. Multidecadal Indian Ocean Variability Linked to the Pacific and Implications for Preconditioning Indian Ocean Dipole Events. *Journal of Climate*, 30(5), pp. 1739-1751. doi:10.1175/JCLI-D-16-0200.1

14. Dong, Lu and McPhaden, M.J., 2016. Interhemispheric SST Gradient Trends in the Indian Ocean Prior to and during the Recent Global Warming Hiatus. *Journal of Climate*, 29(24), pp. 9077-9095. doi:10.1175/JCLI-D-16-0130.1

15. Wang, C., 2019. Three‐Ocean Interactions and Climate Variability: a Review and Perspective. *Climate Dynamics*, 53(7–8), pp. 5119-5136. doi:10.1007/s00382-019-04930-x

16. Chowdary, J.S., Xie, Sh.-P., Tokinaga, H., Okumura, Yu.M., Kubota, H., Johnson, N. and Zheng, X.-T., 2012. Interdecadal Variations in ENSO Teleconnection to the Indo–Western Pacific for 1870–2007. *Journal of Climate*, 25(5), pp. 1722-1744. doi:10.1175/JCLI-D-11-00070.1

17. Li, Y., Han, W., Hu, A., Meehl, G.A. and Wang, F., 2018. Multidecadal Changes of the Upper Indian Ocean Heat Content during 1965–2016. *Journal of Climate*, 31(19), pp. 7863-7884. doi:10.1175/JCLI-D-18-0116.1

18. Han, W., Vialard, J., McPhaden, M.J., Lee, T., Masumoto, Yu., Feng, M. and de Ruijter, W.P., 2014. Indian Ocean Decadal Variability: A Review. *Bulletin of the American Meteorological Society*, 95(11), pp. 1679-1703. doi:10.1175/BAMS-D-13-00028.1

19. Santoso, A., Gupta, A.S. and England, M.H., 2010. Genesis of Indian Ocean Mixed Layer Temperature Anomalies: A Heat Budget Analysis. *Journal of Climate*, 23(20), pp. 5375-5403. doi:10.1175/2010JCLI3072.1

20. Alory, G. and Meyers, G., 2009. Warming of the Upper Equatorial Indian Ocean and Changes in the Heat Budget (1960–99). *Journal of Climate*, 22(1), pp. 93-113. doi:10.1175/2008JCLI2330.1

21. Gong, D. and Wang, S., 1999. Definition of Antarctic Oscillation Index. *Geophysical Research Letters*, 26(4), pp. 459-462. doi:10.1029/1999GL900003

22. Alory, G., Wijffels, S. and Meyers, G., 2007. Observed Temperature Trends in the Indian Ocean over 1960–1999 and Associated Mechanisms. *Geophysical Research Letters*, 34(2)**,** L02606. doi:10.1029/2006GL028044

23. Lyu, K., Zhang, X., Church, J.A. and Wu, Q., 2020. Processes Responsible for the Southern Hemisphere Ocean Heat Uptake and Redistribution under Anthropogenic Warming. *Journal of Climate*, 33(9), pp. 3787-3807. doi:10.1175/JCLI-D-19-0478.1

24. Giglio, D. and Johnson, G.C., 2016. Subantarctic and Polar Fronts of the Antarctic Circumpolar Current and Southern Ocean Heat and Freshwater Content Variability: A View from Argo. *Journal of Physical Oceanography*, 46(3), pp. 749-768. doi:10.1175/JPO-D-15-0131.1

25. Armour, K.C., Marshall, J., Scott, J.R., Donohoe, A. and Newsom, E.R., 2016. Southern Ocean Warming Delayed by Circumpolar Upwelling and Equatorward Transport. *Nature Geoscience*, 9, pp. 549-554. doi:10.1038/ngeo2731

26. Gao, L., Rintoul, S.R. and Yu, W., 2018. Recent Wind-Driven Change in Subantarctic Mode Water and Its Impact on Ocean Heat Storage. *Nature Climate Change*, 8, pp. 58-63. doi:10.1038/s41558-017-0022-8

27. Levitus, S., Antonov, J.I., Boyer, T.P., Baranova, O.K., Garcia, H.E., Locarnini, R.A., Mishonov, A.V., Reagan, J.R., Seidov, D., Yarosh, E.S. and Zweng, M.M., 2012. World Ocean Heat Content and Thermosteric Sea Level Change (0–2000 m), 1955–2010. *Geophysical Research Letters*, 39(10), L10603. doi:10.1029/2012GL051106

28. Häkkinen, S., Rhines, P.B. and Worthen, D.L., 2016. Warming of the Global Ocean: Spatial Structure and Water-Mass Trends. *Journal of Climate*, 29(13), pp. 4949-4963. doi:10.1175/JCLI-D-15-0607.1

29. Mokhov, I.I., Chernokulsky, A.V. and Osipov, A.M., 2020. Atmospheric Centers of Action in the Northern and Southern Hemispheres: Features and Variability. *Russian Meteorology and Hydrology*, 45(11), pp. 749-761. https://doi.org/10.3103/S1068373920110011

30. Rostov, I.D., Dmitrieva, E.V., Rudykh, N.I. and Vorontsov, A.A., 2020. Climatic Changes in Thermal Conditions of Marginal Seas in the Western Pacific. *Russian Meteorology and Hydrology*, 45(3), pp. 169-178. doi:10.3103/S1068373920030048

31. Boyer, T.P., Baranova, O.K., Coleman, C., Garcia, H.E., Grodsky, A., Locarnini, R.A., Mishonov, A.V., Paver, C.R., Reagan, J.R. [et al.], 2018. *World Ocean Database 2018*. NOAA Atlas NESDIS 87. [online] Available at: https://www.ncei.noaa.gov/products/worldocean-database [Accessed: 23 April 2021].

32. Rostov, I.D., Dmitrieva, E.V. and Rudykh, N.I., 2021. Interannual Variability of Thermal Conditions in the Extratropical Zone of the South Pacific at the Turn of the XX–XXI Centuries. *Physical Oceanography*, 28(6), pp. 612-631. doi:10.22449/1573-160X-2021-6-612-631

33. Zhang, Y., Feng, M., Du, Y., Phillips, H.E., Bindoff, N.L. and McPhaden, M.J., 2018. Strengthened Indonesian Throughflow Drives Decadal Warming in the Southern Indian Ocean. *Geophysical Research Letters*, 45(12), pp. 6167-6175. doi:10.1029/2018GL078265

34. Li, Y., Han, W. and Zhang, L., 2017. Enhanced Decadal Warming of the Southeast Indian Ocean during the Recent Global Surface Warming Slowdown. *Geophysical Research Letters*, 44(19), pp. 9876-9884. doi:10.1002/2017GL075050

35. Osipov, A.M. and Gushchina, D.Yu., 2018. El Niño 2015/2016: Evolution, Mechanisms, and Concomitant Remote Anomalies. *Fundamental and Applied Climatology*, (3), pp. 54-81. doi:10.21513/2410-8758-2018-3-54-81 (in Russian).

36. Yang, J., Liu, Q. and Liu, Zh., 2010. Linking Observations of the Asian Monsoon to the Indian Ocean SST: Possible Roles of Indian Ocean Basin Mode and Dipole Mode. *Journal of Climate*, 23(21), pp. 5889-5902. doi:10.1175/2010JCLI2962.1

37. Behera, S.K. and Yamagata, T., 2001. Subtropical SST Dipole Events in the Southern Indian Ocean. *Geophysical Research Letters*, 28(2), pp. 327-330. doi:10.1029/2000GL011451

38. Gupta, A.S. and England, M.H., 2006. Coupled Ocean-Atmosphere-Ice Response to Variations in the Southern Annular Mode. *Journal of Climate*, 19(18), pp. 4457-4486. doi:10.1175/JCLI3843.1

39. Cai, W., 2006. Antarctic Ozone Depletion Causes an Intensification of the Southern Ocean Super-Gyre Circulation. *Geophysical Research Letters*, 33(3), L03712. doi:10.1029/2005GL024911

40. Roemmich, D., Gilson, J., Sutton, P. and Zilberman, N., 2016. Multidecadal Change of the South Pacific Gyre Circulation. *Journal of Physical Oceanography*, 46(6), pp. 1871-1883. doi:10.1175/JPO-D-15-0237.1

About the authors:

Igor D. Rostov, Head of the Laboratory of Informatics and Ocean Monitoring, V. I. Il'ichev Pacific Oceanological Institute. Far Eastern Branch of Russian Academy of Sciences (43 Baltiyskaya str., Vladivostok, 690041, Russian Federation), Ph.D. (Geogr.), **ORCID ID: 0000-0001-5081-7279**, rostov@poi.dvo.ru

Elena V. Dmitrieva, Senior Research Associate, Laboratory of Informatics and Ocean Monitoring, V. I. Il'ichev Pacific Oceanological Institute. Far Eastern Branch of Russian Academy of Sciences (43 Baltiyskaya str., Vladivostok, 690041, Russian Federation), Ph.D. (Tech.), **ORCID ID: 0000-0002-0094-5296**, e_dmitrieva@poi.dvo.ru

Natalia I. Rudykh, Senior Research Associate, Laboratory of Informatics and Ocean Monitoring, V. I. Il'ichev Pacific Oceanological Institute. Far Eastern Branch of Russian Academy of Sciences (43 Baltiyskaya str., Vladivostok, 690041, Russian Federation), Ph.D. (Geogr.), **ResearcherID: N-5821-2018**, rudykh@poi.dvo.ru

Contribution of the co-authors:

Igor D. Rostov – development of the article structure, processing, and analysis of the data, writing the article text

Elena V. Dmitrieva – collection and processing of oceanographic data, calculations, drawing design, text editing

Natalia I. Rudykh – collection and processing of initial data on meteorological stations, calculations, editing of text, and references

All the authors have read and approved the final manuscript.
The authors declare that they have no conflict of interest.